

bradscholars

Seismic response of prestressed precast reinforced concrete beam-column joints assembled by steel sleeves

Item Type	Article
Authors	Xue, H.;Ashour, Ashraf;Ge, W.;Cao, D.;Sun, C.;Cao, S.
Citation	Xue H, Ashour AF, Ge W et al (2023) Seismic response of prestressed precast reinforced concrete beam-column joints assembled by steel sleeves. Engineering Structures. 276: 115328.
DOI	https://doi.org/10.1016/j.engstruct.2022.115328
Publisher	Elsevier
Rights	© 2022 Elsevier. Reproduced in accordance with the publisher's self-archiving policy. This manuscript version is made available under the CC-BY-NC-ND 4.0 license (https://creativecommons.org/licenses/by-nc-nd/4.0)
Download date	2026-06-11 00:42:34
Link to Item	http://hdl.handle.net/10454/19203

24 **Keywords:** beam-column joint; steel sleeve; prestressed precast; seismic performance; shear
25 capacity

26 **1. Introduction**

27 In a seismic event, beam-column joints are the most crucial component in reinforced
28 concrete (RC) frame structure, playing a significant role in transferring internal forces between
29 beams and columns. Therefore, a reliable and effective design of beam-column joints is
30 particularly important to ensure the safety of structures [1-5]. Precast RC beam-column joints
31 have many advantages, in comparison with traditional in-situ RC joints, such as faster
32 construction, high production efficiency, less onsite wet work, less waste, and high-quality
33 assurance and standardization of components. Furthermore, the use of prestressed
34 reinforcement ensures the integrity of joints, inhibits crack development, and enhances post-
35 earthquake recovery [6-8]. Therefore, prestressed precast RC beam-column joints are widely
36 used in various structures, and their mechanical performance is the focus of many research
37 investigations [9].

38 There are usually two structural types of precast RC joints: wet and dry connections. In
39 dry connections, the precast structural elements are directly connected to each other and no
40 cast-in-place concrete is used, achieving many advantages such as convenient connection,
41 better assembly degree, and higher construction efficiency [10-11]. Over the past decades, a
42 considerable number of prestressed precast assembly RC joints have been proposed and their
43 proof of concept has been experimentally investigated. For example, Korkmaz et al. [12]
44 proposed a new type of precast concrete beam-column connections with a cantilevered beam
45 extending a certain length out from the side of the column, in which the reinforcements at the
46 top and bottom of the precast beam were welded firmly to the cantilevered reinforcement, and
47 concrete was cast at the connection site. The test results showed that the new precast concrete
48 beam-column joint has a larger bearing capacity and stiffness than traditional cast-in-place

49 joints. Kim et al. [13] investigated the seismic performance of prestressed precast RC beam-
50 column joints using the post-tensioning technique, which exhibited a good structural seismic
51 performance. Cai et al. [14, 15] proposed a new prestressed precast beam-column joint
52 assembled with unbonded post-tensioned prestressing tendons, bolts, and angles. The effect of
53 initial prestressing on the seismic performance of such joints was investigated, demonstrating
54 the reliability of the post-tensioned prestressing tendons in the application of precast joints.
55 Vidjeapriya et al. [16] conducted an experimental study on the seismic performance of precast
56 RC beam-column joints consisting of a bull leg and ribbed angles, connecting the precast
57 concrete beam-column into a single unit by means of angles and bolts. The test results showed
58 that the ductility and energy dissipation capacity of the proposed precast joints outperform those
59 of the cast-in-place joints. The above studies show that, the assembled joints connected by
60 prestress tendons have good self-centring ability and shear capacity. The application of steel
61 plates can improve ductility and enhance the seismic performance of precast joints.

62 Bolted dry connections are equally effective in meeting the structural integrity and strength
63 of joints. Erats et al. [17] performed low cycle loading test on five specimens of precast RC
64 bolted and welded connections, and found that, compared with the welded joints, the bolted
65 joints are superior in bearing capacity, energy dissipation capacity, ductility, construction and
66 production. Nakaki [18] and Englekirk [19] proposed a bolt-high ductility joint with high
67 deformation capacity and less damage compared to cast-in-place joints, they reported the failure
68 mode of the joint is not so significant when the interlayer displacement reaches 3.5%. Liu et al.
69 [20] designed a new type of precast RC beam-column joint, which is connected by bolts and
70 welding, and this bolted beam-column joint has a higher load-bearing capacity compared to
71 cast-in-place joints. Choi et al. [21] proposed an RC beam-column joint using steel plates,
72 bolted connections and post-cast engineered cementitious composite (ECC), which was studied
73 in a quasi-static experiment. The results showed that the joint has a better load capacity and

74 ductility than the cast-in-place joint. Bai et al. [22] proposed a novel precast replaceable RC
75 joint with high-strength bolts at steel beam-column connectors, that experimentally exhibited
76 satisfactory energy dissipation capacity and hysteretic behavior. The above studies show that
77 the precast joints connected by bolts are efficient in construction and satisfy the seismic
78 performance of the joints. However, the effect of bolts on the self-centring ability and stiffness
79 of joints is not considered.

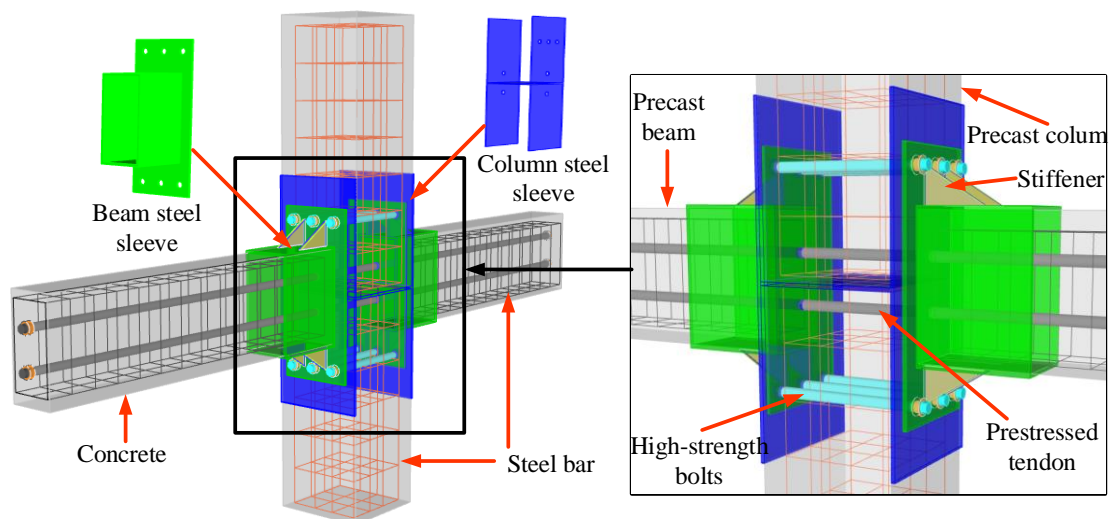
80 In order to improve the energy dissipation capacity, ductility and assembly efficiency of
81 prestressed precast RC joints, a new type of prestressed precast RC beam-column joint
82 assembled by steel sleeves is proposed in this paper. The steel sleeve stiffeners could resist the
83 action of positive and negative bending moments. The prestressed tendons penetrating the
84 precast beams and columns were stretched using the post-tensioning method, ensuring the joint
85 integrity and providing excellent post-earthquake recovery ability. The influence of the design
86 parameters, including the axial compression ratio, stirrup ratio and effective prestress
87 established at the end of the beam, on the seismic performance and shear capacity of the new
88 type of joint is studied. A method to evaluate the shear capacity of the prestressed precast RC
89 beam-column joints assembled by the steel sleeves is also proposed and verified by the
90 experimental results.

91 **2. Experimental program**

92 **2.1. Details of the proposed connection**

93 The connection details of the test specimens are shown in Fig. 1. The prestressed precast
94 RC joints assembled by steel sleeves had the same dimensions as the cast-in-place RC joints.
95 The prestressed precast RC joints assembled by steel sleeves consisted of five parts: the precast
96 RC beams, the precast RC columns, the beam steel sleeves, the column steel sleeves, and the
97 prestressed tendons. The proposed joint can be quickly assembled on site by the restraint of the
98 steel sleeves, prestressed strands and high-strength bolt connections. As the cross-sections of

99 the precast beams were slightly smaller than the inner dimensions of the steel jacket of the beam
100 end extension, grouting joints were reserved between the concrete and steel sleeve, and a high-
101 strength grout was injected to form an effective bond between the concrete and the steel sleeve.
102 The steel sleeves were aligned with the holes in the column body, high-strength bolts were, then,
103 used to secure the steel sleeves in place, and high-strength grouts were injected into the steel
104 sleeves. Finally, the high-strength bolts were tightened after curing. The fabrication process of
105 the specimens tested is shown in Fig. 2. In order to enhance the slip resistance of the steel-
106 concrete interface, a certain number of shear pins were welded on the inner side of the beam
107 steel sleeve [23]. The bubble paper, bone-dewing agent, and chiseling were also adopted to
108 increase the roughness of the concrete surface in the inserted part, so that the steel sleeve and
109 the concrete could maintain good connectivity and integrity. After positioning and aligning the
110 bolt and the prestressing apertures, high-strength friction-type bolts were installed for assembly
111 and fixing, followed by tensioning the prestressed tendons through the reserved prestressing
112 apertures to ensure that the prestressed tendons were in an elastic state during loading, so that
113 the joints had a certain safety reserve.



114
115

Fig. 1. Details of the interior connections.



116

117

(a) Precast column steel sleeve

(b) Precast beam steel sleeve

(c) Concrete pouring



118

119

120

(d) Precast beam assembly

(e) Precast column assembly

(f) Assembled specimen

Fig. 2. Specimen preparations.

121

122

2.2. Specimen design

123

124

125

126

127

128

129

130

131

132

133

134

135

136

A total of five specimens were prepared and tested under cyclic loading, including four prestressed precast RC joints assembled by steel sleeves and one cast-in-place RC joint, marked as ZJ-1, ZJ-2, ZJ-3, ZJ-4 and XJ-1, respectively. The tests were conducted to study the influences of the axial compression ratio, stirrup ratio in the core area, and effective prestress established at the end of the beam. The axial compression ratio (N/N_y) is defined as the applied axial load (N) to the yield strength of the entire column section (N_y). The effective prestress is the stress remaining in the prestressed tendon after some prestress loss occurred. The design of joint specimens was based on the design standards of GB 50011-2010 [24], JGJ 138-2016 [25] and GB 50017-2010 [26]. The economical reinforcement ratios of beams and columns in frames are 0.6%~1.5%; and 0.6%~3.0%, respectively, whereas the maximum reinforcement ratio of columns is 5.0% [27]. The steel reinforcements of beams and columns in the current investigation were selected on the higher side to allow a larger capacity of connections and a wider range of loading and behaviour. Therefore, three reinforcing bars with diameter of 25 mm (reinforcement ratio = 2%) were provided at the top and bottom of the beam cross section,

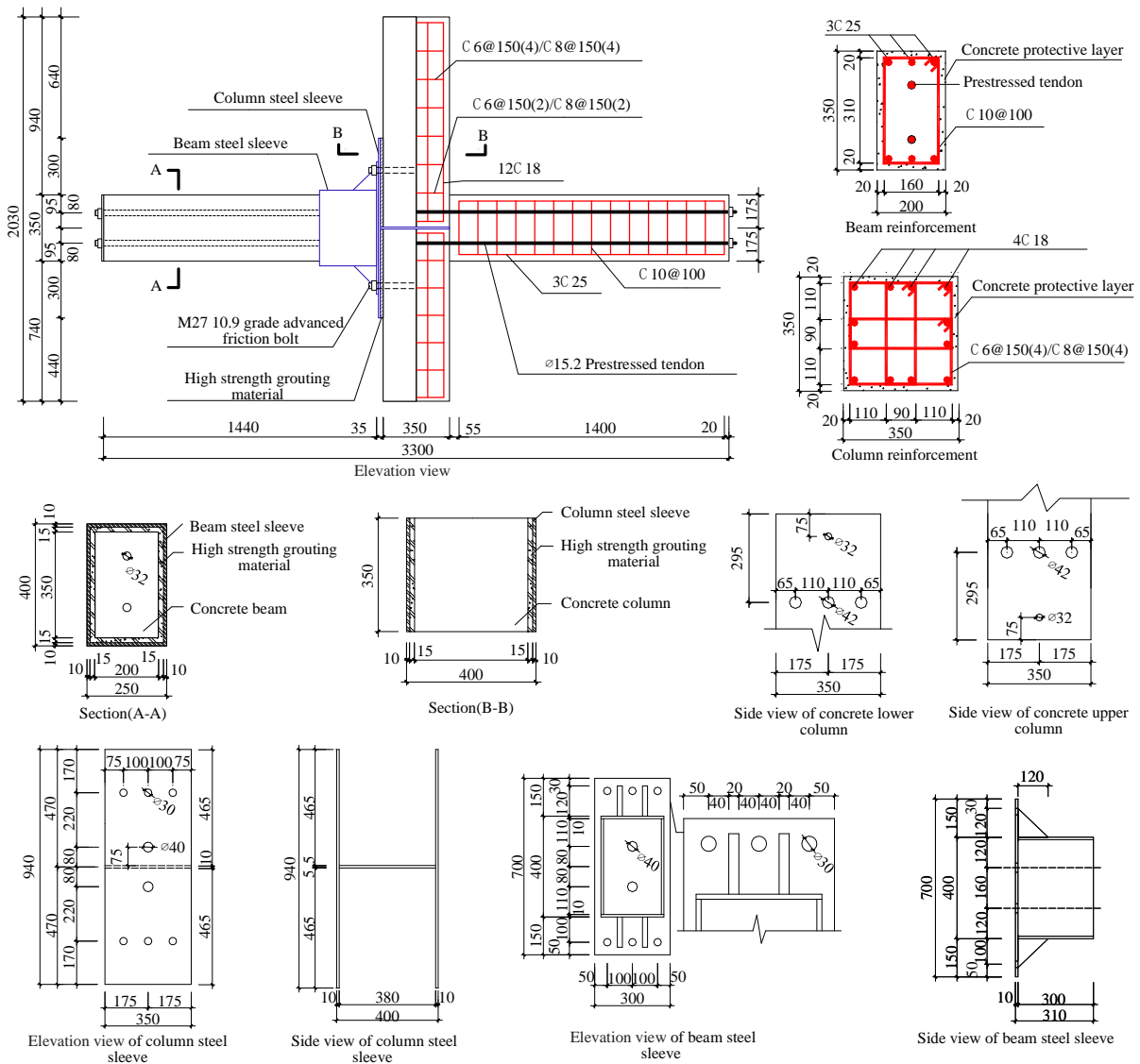
137 whereas twelve reinforcing bars of 18 mm diameter (reinforcement ratio=2.5%) were uniformly
 138 distributed in the column section as shown in Fig. 1. It is also to be noted that the section of
 139 column was designed to be stronger than that of beam, ensuring ductile behaviour of connection
 140 and easier retrofitting after earthquakes. Table 1 shows the design parameters of the specimens
 141 tested.

142 **Table 1** Parameters of the specimens tested

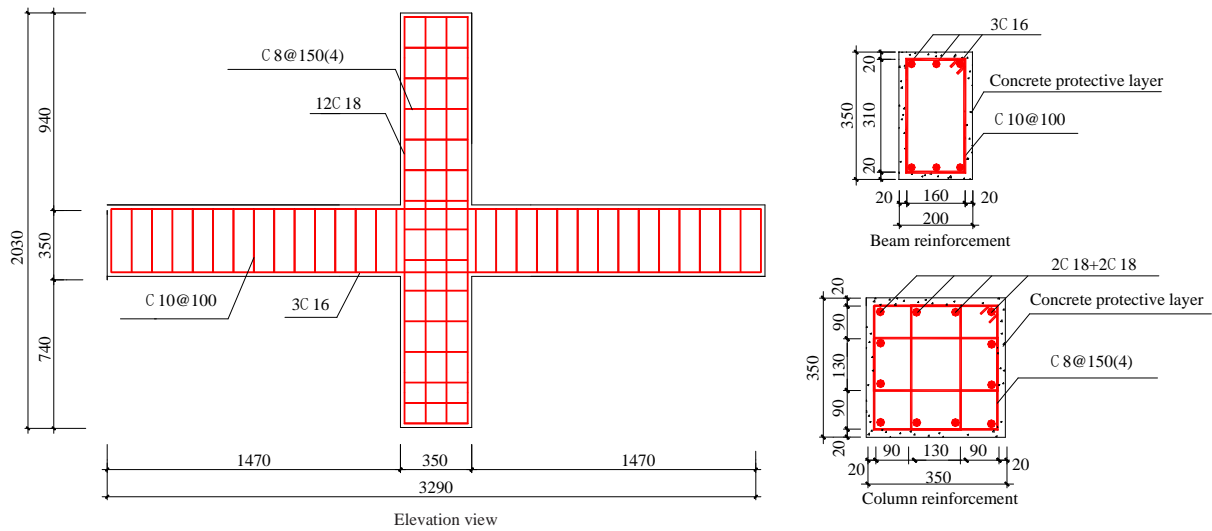
Specimen	Type	Axial compression ratio	Stirrup ratio (%)	Bolt diameter (mm)	Steel plate thickness (mm)	Effective prestress (MPa)
ZJ-1	Precast	0.1	0.12	27	10	636.9
ZJ-2	Precast	0.2	0.12	27	10	656.3
ZJ-3	Precast	0.1	0.12	27	10	926.5
ZJ-4	Precast	0.1	0.21	27	10	694.8
XJ-1	Cast-in-place	0.1	0.21	—	—	—

143 The geometric dimensions and reinforcement details of all specimens are shown in Fig. 3.
 144 The length and height of the specimens ZJ-1 to ZJ-4 were 3300 mm and 2030 mm respectively,
 145 while the length and height of specimen XJ-1 were 3290 mm and 2030 mm respectively. The
 146 concrete cover thickness of the steel reinforcement was 20 mm. The dimension of the reinforced
 147 concrete beam cross-section of all specimens was 200 mm × 350 mm. The length of both the
 148 left and right beams of specimens ZJ-1 to ZJ-4 was 1440 mm, and that of specimen XJ-1 was
 149 1470 mm. The precast RC column had a square section of 350 mm × 350 mm, a height of the
 150 upper column of 1110 mm, and a height of the lower column of 910 mm. The diameter of the
 151 prestressed orifice on the RC beam and column was 32 mm, and the diameter of the prestressed
 152 orifice for the bolts on the column was 42 mm. HRB400 grade steel reinforcements were used
 153 for all the specimens. Two diameters of 25 mm and 16 mm were used for the longitudinal
 154 reinforcements in the concrete beam. The diameter of the stirrups was 10 mm, and the
 155 prestressed tendon was ϕ_s 15.2. The RC column was reinforced with 12 longitudinal steel bars
 156 with a diameter of 18 mm and lateral stirrups with diameters of 6 mm and 8 mm. Q235 grade
 157 steel was used for the steel sleeves. The beam steel sleeve consisted of a flange plate, a beam

158 extension sleeve and a stiffener. The dimension of the stiffener was 120 mm × 120 mm, and the
 159 thickness was 20 mm. The thickness of the steel sleeve was 10 mm. The column steel sleeve
 160 consisted of a flange plate and an internal horizontal spacer. The total height of the column steel
 161 sleeve was 940 mm, and the section size was 350 mm × 400 mm. The section size of the beam
 162 sleeve was 250 mm × 400 mm, and the length was 300 mm. The diameter of the reserved holes
 163 for the bolts on the beam and column steel sleeve was 40 mm, and the diameter of the reserved
 164 holes for the prestressed tendons was 30 mm. Six 10.9 grade M27 high-strength friction bolts
 165 were used.



(a) Details of specimens ZJ-1, ZJ-2, ZJ-3, and ZJ-4.



(b) Details of specimen XJ-1

Fig. 3. Dimensions and details of test specimens (unit: mm).

2.2. Material properties and testing procedure

Grade C40 concrete was used for all test specimens. The mix proportion of concrete is presented in Table 2. Six groups of 150 mm × 150 mm × 300 mm concrete prism specimens were fabricated and cured for 28 days to obtain the axial compressive strength and elastic modulus according to GB/T 50081-2019 [28]. Additionally, the 28-day compressive strength was measured for three 100-mm concrete cubes. The test results were summarized in Table 3.

Table 2 Concrete mix proportion

Water (kg/m ³)	Sand (kg/m ³)	Cement (kg/m ³)	Gravel (kg/m ³)	Water-to-cement ratio
185	533	487	1245	0.41

Table 3 Concrete properties

Specimen	Cube compressive strength	Axial compressive strength	Modulus of elasticity
	(MPa)	(MPa)	
C40	42.8	28.9	32.3
	41.9	27.6	32.1
	42.6	27.5	32.5

The steel plates, prestressed tendons, and reinforcements were tested according to GB 228.1-2021 [29], and the mechanical properties of these materials are listed in Table 4.

Table 4 Material properties of steel materials

Components	Diameter(mm)	Yield strength	Ultimate strength	Elastic modulus
		(MPa)	(MPa)	(GPa)

Steel plate	—	314.1	483.3	206.0
Prestressed tendon	15.2	—	1930.2	195.0
M27 bolt	27.0	900.0	1000.0	211.0
	6.0	421.4	539.3	200.0
	8.0	445.2	602.7	200.0
Steel bars	10.0	436.5	594.1	200.0
	16.0	451.3	587.3	200.0
	18.0	442.5	593.2	200.0
	25.0	455.7	603.6	200.0

182 Fig. 4 shows the joint assembly test rig. Before the joint loading, a 1900kN capacity
183 hydraulic jack was used to apply constant vertical pressure at the top of the column. The axial
184 load applied to the column specimen was determined according to the axial compression ratio
185 of the specimen and was kept constant throughout the loading process as monitored by a load
186 sensor. At the end of the column, an actuator with a capacity of 500kN was used to apply a
187 reciprocating displacement. The horizontal load and displacement at the end of the column were
188 recorded by an actuator data acquisition system. The axial deformation of the column under
189 load is calculated from the recorded displacement of the actuator minus the slip at the bottom
190 that is measured by a displacement gauge located at the column end of the specimen. The
191 loading regime prescribed by JGJ/T 101-2015 [30] was adopted. As shown in Fig 5, a mixed
192 load-displacement control method was utilized. At the beginning of the test, a load-control
193 mode was adopted, and the load amplitude of each loop was set as 30%, 75% and 100% of the
194 initial yield load, and each load level was applied only once. When the yield load was reached,
195 displacement-control mode was used. The applied displacement at each cycle was
196 incrementally increased, such as Δ_y , $2\Delta_y$, $3\Delta_y$, ..., $n\Delta_y$, and each displacement level was repeated
197 three times until the specimen failed.

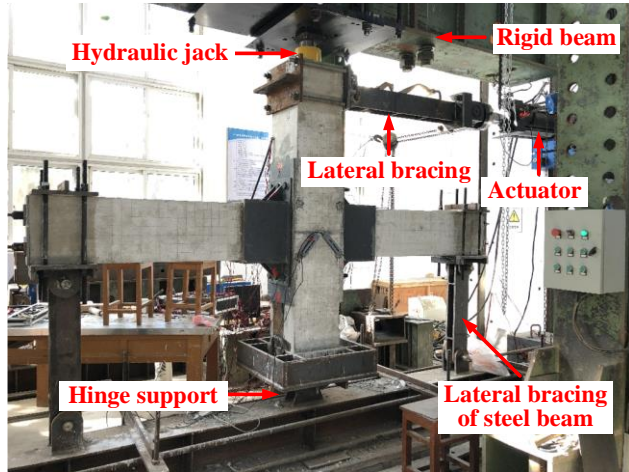


Fig. 4. Test setup.

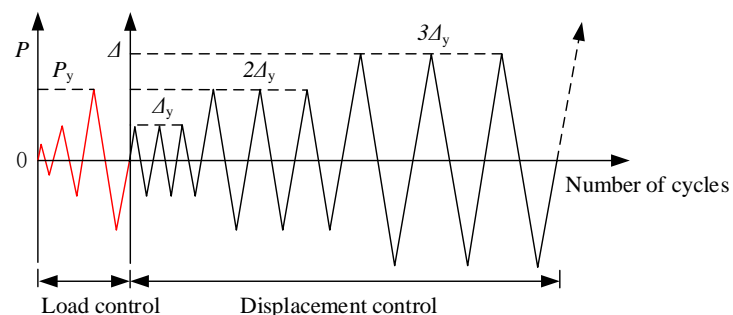
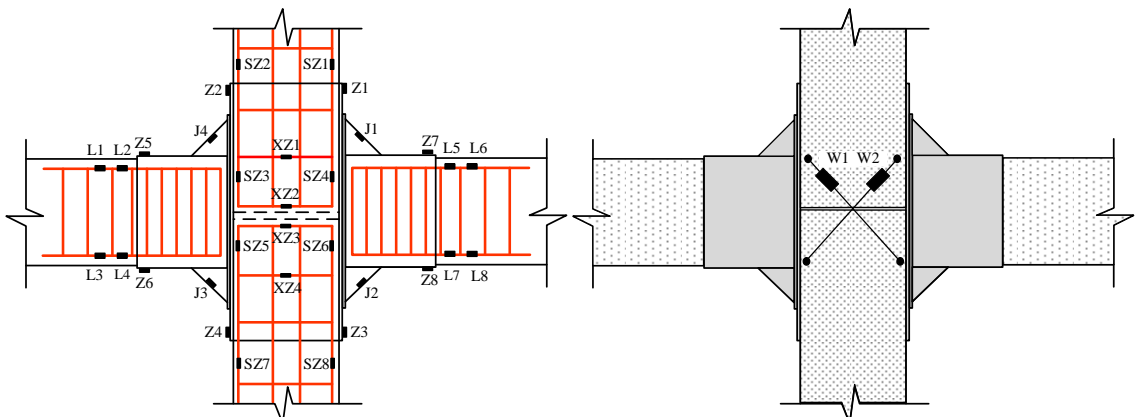


Fig. 5. Cyclic loading system.

Fig. 6 shows the location of 32 strain gauges and 2 LVDTs to monitor strains and displacements at the selected positions. The sensitivity and measurement range of LVDTs are 0.2 mv/mm and 100 mm, respectively. The strain gauges on stiffeners, column steel sleeves, beam steel sleeves, beam longitudinal reinforcement bars, column longitudinal reinforcement bars, and stirrups in the joint core area were numbered J1-J4, Z1-Z4, Z5-Z8, L1-L8, SZ1-SZ8 and XZ1-XZ4, respectively.



209
210
211
212
213
214
215
216
217
218
219
220
221
222
223
224
225
226
227
228
229

(a)

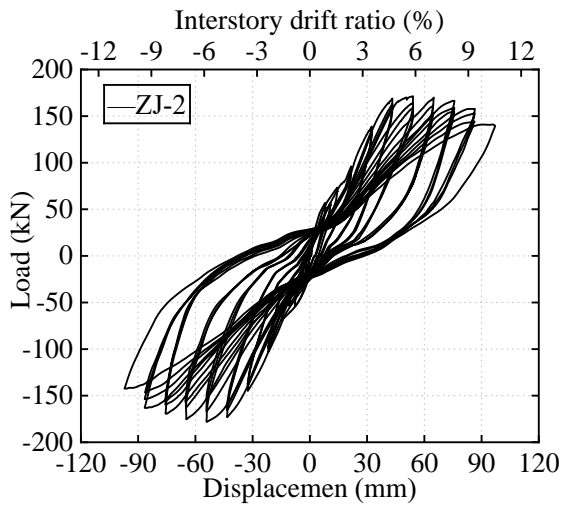
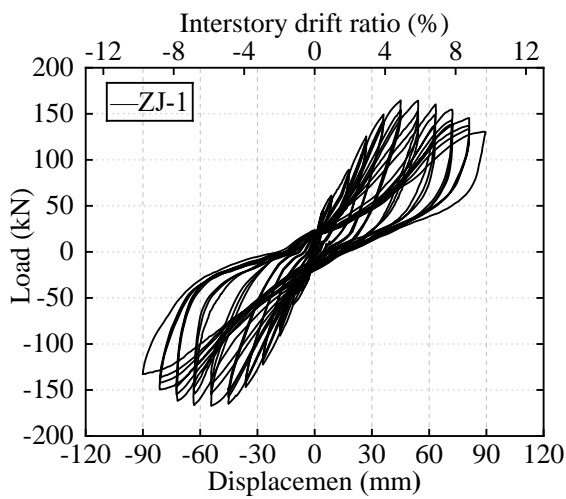
(b)

Fig. 6 Layout of LVDTs and strain gauges of specimens: (a) layout of strain gauges, (b) layout of LVDTs.

3. Experimental results and discussions

3.1. Load-displacement curves

Fig. 7 shows the horizontal load-displacement relationship of the five beam-column joints. As can be seen, both the initial stiffness and horizontal bearing capacity of the specimens ZJ-1, ZJ-2, ZJ-3, and ZJ-4 are larger than those of specimen XJ-1, and they show better linear elastic behavior at the initial stage of loading. In addition, the overlap of the hysteresis curves of each loading cycle of specimens ZJ-1, ZJ-2, ZJ-3 and ZJ-4 is better than that of specimen XJ-1, indicating that the recovery performance of prestressed precast RC joints assembled by steel sleeves is better than that of the cast-in-place one, but the hysteresis curve of cast-in-place specimen XJ-1 is fuller than that of specimens ZJ-1, ZJ-2, ZJ-3 and ZJ-4. Compared with specimen ZJ-1, the horizontal bearing capacity of specimen ZJ-2 is improved. The deformation of the core area is relatively small, and the pinched phenomenon is improved, confirming that the increase in axial compression ratio inhibits the development of core diagonal cracks to a certain extent. Under the same conditions, specimen ZJ-3 shows an increase in initial stiffness, horizontal yield load, and horizontal ultimate load compared with specimen ZJ-2 because of the increase in prestress. For the specimen ZJ-4, the cyclic hysteresis curve is fuller, and the stiffness and strength degradation are relatively smaller, indicating that the increase of the stirrup ratio in the core area of the joint improves the ductility of the prestressed precast RC joint assembled by steel sleeves.

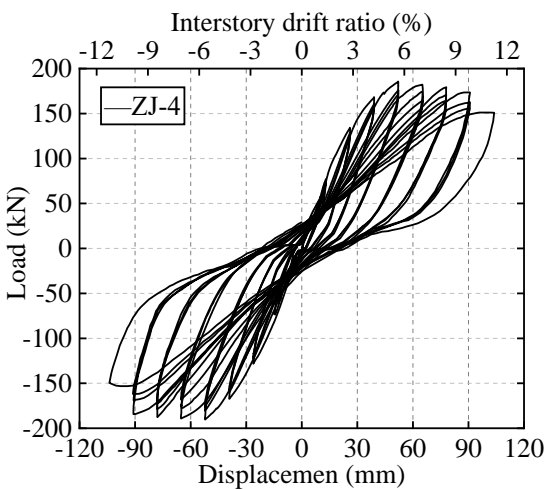
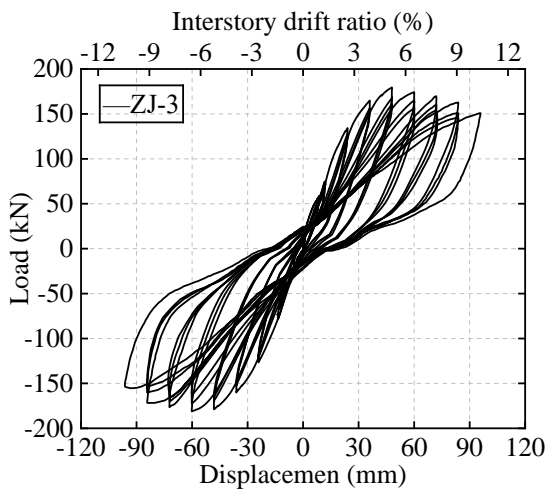


230

231

(a)

(b)

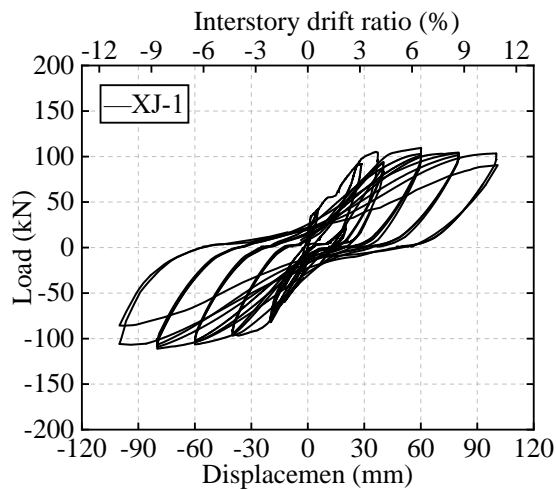


232

233

(c)

(d)



234

235

(e)

236 **Fig. 7.** Horizontal load-displacement hysteresis curves for (a) ZJ-1, (b) ZJ-2, (c) ZJ-3, (d) ZJ-4, and (e) XJ-

237

1 joints.

238 **3.2. Envelope curves**

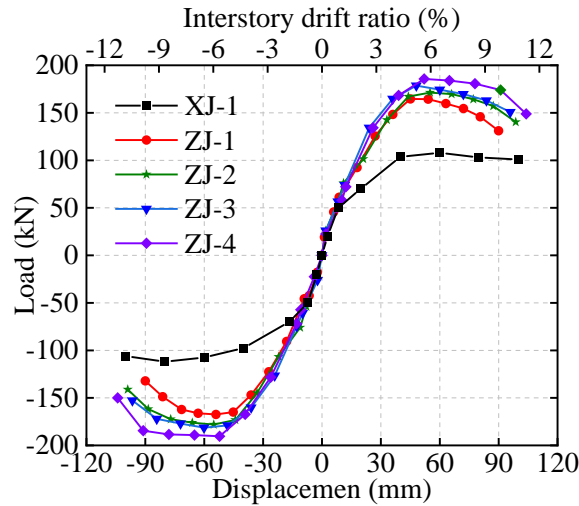
239 Fig. 8 shows the envelope curves of the beam-column joints. Table 5 lists the horizontal
 240 yield displacement Δ_y , horizontal ultimate displacement Δ_u , and displacement ductility ratio μ
 241 of the beam-column joints tested. The positive peak bearing capacity P_m of specimen ZJ-1 is
 242 164.5 kN, which is 52.0% higher than that of the cast-in-place specimen XJ-1. The horizontal
 243 ultimate displacement is reduced by 10.1% due to the effect of prestressed tendons and steel
 244 sleeve stiffeners. Compared with specimen ZJ-1, the maximum horizontal bearing capacity and
 245 horizontal ultimate displacement of specimen ZJ-2, subjected double the axial compression
 246 ratio of 0.2, increased by 4.1% and 9.0%, respectively. Compared with the specimen ZJ-1, the
 247 maximum horizontal bearing capacity of the specimen ZJ-3 increased by 8.6%, the horizontal
 248 ultimate displacement increased by 6.6%, the shear bearing capacity of the core area of the
 249 prestressed precast RC joint assembled by steel sleeves was significantly improved, and the
 250 ductility was better. The results indicate that the increase of effective prestress established at
 251 the end of the beam improves the shear resistance of the prestressed precast RC joints assembled
 252 by steel sleeves. As the stirrup ratio in the core zone of specimen ZJ-4 is 0.21%, the horizontal
 253 peak bearing capacity is 12.8% and 72.0% higher than these of specimen ZJ-1 and specimen
 254 XJ-1, respectively. The horizontal ultimate displacement is 4.0% higher than that of specimen
 255 XJ-1, and the post-peak bearing capacity degrades relatively slowly. It can be observed that,
 256 the restraining effect of the stirrup on the core area is more efficient than that of prestressed
 257 tendons. It can be seen from Fig. 8, the stiffness of the specimens ZJ-1 to ZJ-4 is greater than
 258 that of specimen XJ-1. The main reason is the final failure modes of all prestressed precast RC
 259 joints assembled by steel sleeves are shear failure rather than bending failure.

260 **Table 5** Test results

Specimen	Direction	P_y (kN)	Δ_y (mm)	P_{max} (kN)	P_u (kN)	Δ_u (mm)	μ	$\bar{\mu}$
ZJ-1	Positive	134.7	31.8	164.5	131.1	90.0	2.83	2.82
	Negative	139.1	32.2	167.5	132.2	90.1	2.80	
ZJ-2	Positive	148.9	36.6	171.3	140.2	98.1	2.68	2.67

Specimen	Direction	P_y (kN)	Δ_y (mm)	P_{max} (kN)	P_u (kN)	Δ_u (mm)	μ	$\bar{\mu}$
ZJ-3	Negative	154.8	37.2	178.4	141.2	98.9	2.66	2.79
	Positive	155.9	33.4	178.6	150.7	96.0	2.87	
ZJ-4	Negative	155.6	35.7	181.4	152.8	96.6	2.71	
	Positive	161.3	36.5	185.6	148.8	104.1	2.86	
XJ-1	Negative	163.0	36.7	190.4	150.1	105.1	2.87	2.87
	Positive	90.6	31.2	107.9	100.9	100.1	3.21	
XJ-1	Negative	93.4	35.2	107.9	106.1	99.9	2.84	3.03

261



262

263

Fig. 8. Skeleton curves.

264

265

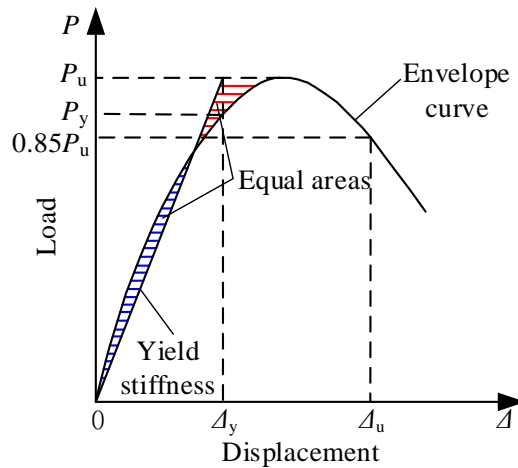
266

267

268

269

The horizontal ultimate displacement Δ_u is defined as the horizontal displacement when the horizontal load decreased to 85% of the peak value. At the time of specimen failure, the horizontal load does not drop below 85% of the peak point load in the skeleton curve, and the corresponding displacement is taken as the horizontal ultimate displacement. The horizontal yield displacement Δ_y and the horizontal yield load P_y of the specimen are determined based on the equal energy principle [31] as shown in Fig 9.



270

271

Fig. 9. Definitions of horizontal yield displacement and horizontal ultimate displacement [31].

272

3.3. Strains in steel reinforcement and plates

273

274

275

276

277

278

279

280

281

282

283

284

285

The test results show similar trends in the strain at the same measuring points of different test specimens. In this paper, only the yielding procedure in different parts of specimen ZJ-1 is evaluated. Fig. 10 shows the strain in the steel sleeves, stiffeners, longitudinal reinforcement bars and stirrups of the joint core area of specimen ZJ-1 versus the applied lateral displacement. From the figure, the strain in the steel sleeves and stiffeners did not reach the yield strain at the end of loading. The compressive strain did not occur in the strain gauge Z7. This is due to the relatively small width-to-thickness ratio of the beam steel sleeves, the local buckling of the steel plate occurs locally during negative loading, which is consistent with the test results. In Fig. 10(c), all stirrups in the joint core area yielded, thereby, indicating shear failure in the joint core area, as previously outlined. The strain of strain gauge XZ4 is larger than that of strain gauge XZ3. It can be seen, the shear force in the middle of the joint core area is the largest. In Fig. 10(d), for most of the longitudinal reinforcement bars, the strains of specimen ZJ-1 increase along with the increasing lateral displacement, and do not reach the yield strain of 0.0022.

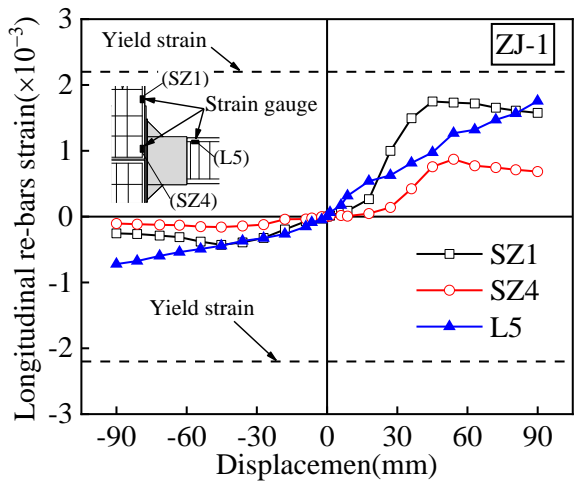
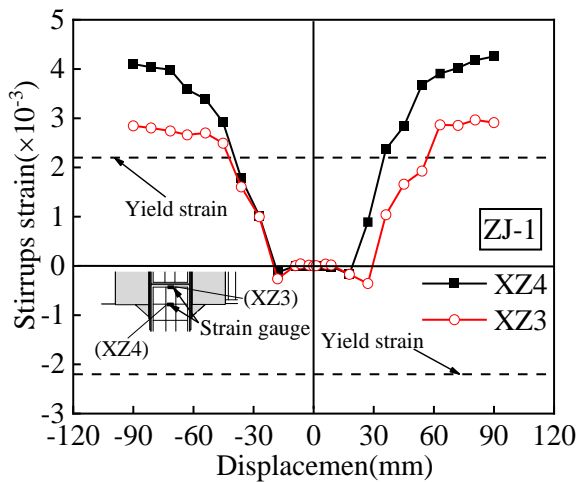
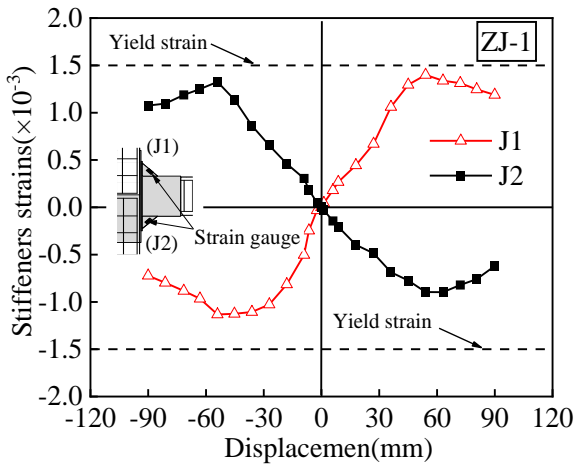
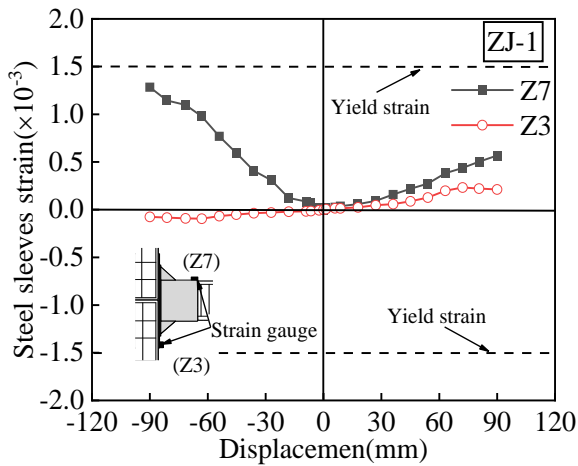


Fig. 10. Strain profiles of specimen ZJ-1.

3.4. Failure patterns

In order to study the failure pattern of the precast joint, the steel reinforcement of beams was selected on the higher side to promote failure at the joint, rather than the beam or column. The failure patterns and overall cracking patterns of the joints tested are shown in Fig. 11. Specimens ZJ-1 to ZJ-4 exhibited shear failure in the core area of the joint, while specimen XJ-1 showed bending failure at the beam end, agreeing well with their initial design. The crack propagation and failure process of all specimens can be divided into four main stages. a) Elastic stage: no cracks were observed in concrete at all joints core; b) Yield stage: diagonal cracks were observed at the core concrete of the joints ZJ-1 to ZJ-4 but stirrups did not yield. The cracks gradually propagated and penetrated through the beam component of the joint XJ-1, and

301 were not completely closed when reverse loading was applied; c) Ultimate strength state: the
302 steel sleeves and longitudinal reinforcements of the joints ZJ-1 to ZJ-4 were not yielded, while
303 stirrups yielded. The concrete cracks development in the core area of the joints ZJ-1 to ZJ-4
304 were significant, accompanied with peeling off the concrete at the surface. The compression
305 zone of the concrete beam of the joint XJ-1 was slightly crushed, and the longitudinal
306 reinforcements reached the yield stress, indicating that the ultimate load of the joint was reached;
307 d) Failure stage: both the width and length of diagonal cracks in the concrete of the core area
308 of the joints ZJ-1 to ZJ-4 significantly increased with tearing sounds and concrete in the core
309 area seriously spalled out, leaving the steel bars exposed. The concrete fragments of the
310 concrete beam of the joint XJ-1 began to fall off from the beam end, and the longitudinal
311 reinforcements and stirrups of the beam end were also exposed. The horizontal bearing capacity
312 of the column end decreased, and the specimen failed.

313 On the other hand, the shear failure process of the specimens ZJ-1 to ZJ-4 may be divided
314 into four stages: initial crack, through a crack, ultimate state, followed by failure. In the initial
315 crack stage, when the load reached 50% to 80% of the peak load, the first diagonal crack
316 occurred on the upper and lower concrete surfaces of the core area of the specimens ZJ-1 to ZJ-
317 4. The core area of the specimens ZJ-1 to ZJ-4 entered the through-crack stage as the load
318 proceeded. At this time, the cracks in the diagonal direction developed rapidly, and the initial
319 diagonal cracks generated in the initial stage became two orthogonal ones extending to the
320 diagonal corners. The main diagonal cracks ran through the surface of the core area of
321 specimens ZJ-1 to ZJ-4, and many short cracks parallel to the main diagonal crack occurred.
322 The concrete surface at the core area was in rhombic grid shapes. As the test loading continued,
323 the specimens ZJ-1 to ZJ-4 entered the ultimate stage. The expansion rate of the width of the
324 main crack accelerated, and a peeling phenomenon was observed in the local area of the
325 concrete. The original cross diagonal cracks of specimens ZJ-1 to ZJ-4 developed significantly,

326 and the concrete at the intersection of the main cracks gradually produced spalling. At the failure
327 stage, the cross cracks in the core area of specimens ZJ-1 to ZJ-4 continued to develop. The
328 shear deformation of specimens ZJ-1 to ZJ-4 increased rapidly, and the concrete near the main
329 diagonal cracks made a tearing sound and spalled severely.

330 There are many cracks in the core area of specimen ZJ-2, and the angle between the
331 diagonal cracks and the horizontal direction was slightly larger. The degree of spalling damage
332 was not as serious as that of specimen ZJ-1. The main reason is that a larger axial pressure
333 increases the angle between the principal compressive stress and the horizontal direction in the
334 joint core area and decreases the angle between the principal tensile stress and the horizontal
335 direction, which results in the change of the inclination angle of the diagonal cracks. On the
336 other hand, the increase of the axial pressure in a certain range could increase the area of the
337 cross-sectional compression zone of the column, strengthen the action of the diagonal
338 compression strut of the concrete in the core area, and enhance the occlusion force between the
339 concrete blocks in the case of concrete cracks, thus improving the shear capacity in the core
340 area of the joint.

341 Compared with specimen ZJ-1, specimen ZJ-3 had better core area and beam crack closure
342 after unloading, and ZJ-3 had a higher initial stiffness, cracking load and ultimate load due to
343 the prestressing acting as a restraint on the two-way stress state.

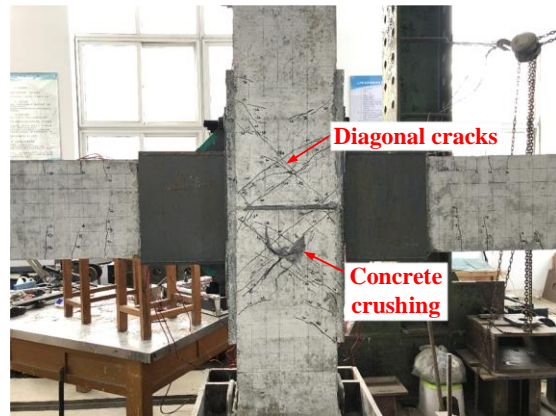
344 Compared with specimen ZJ-1, the cracking load of specimen ZJ-4 was slightly larger,
345 and the width of the cracks was relatively smaller. As the stirrup ratio of specimen ZJ-4 was
346 higher than that of specimen ZJ-1, its cracks were less and developed more slowly, indicating
347 that the shear capacity of the joints could be improved by appropriately increasing the stirrup
348 ratio of the core area of joints in the design stage.

349 The failure mode of specimen XJ-1 was the bending failure of the beam end. Since the
350 beam end was mainly affected by the bending moment, bending cracks were first generated.

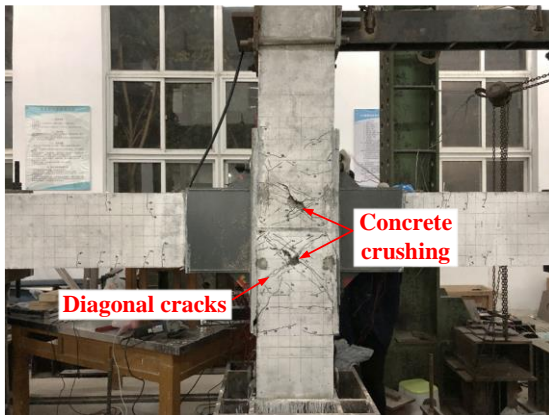
351 When the test loading was increasing step by step, the cracks at the beam end developed and
352 extended from the bottom and top of the beam to the neutral layer respectively, and finally
353 formed a crack penetration state. A small number of cracks appeared in the core area of
354 specimen XJ-1, but the cracks were relatively subtle, which was because when the joint was
355 subjected to a small load, the longitudinal reinforcement in the beam yielded and the shear force
356 transferred to the joint was small, which did not cause the joint to shear damage.



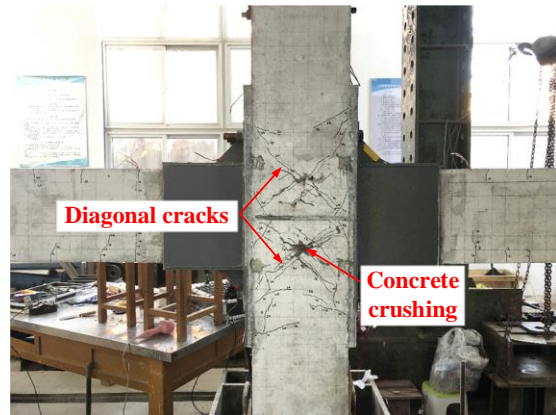
(a) ZJ-1



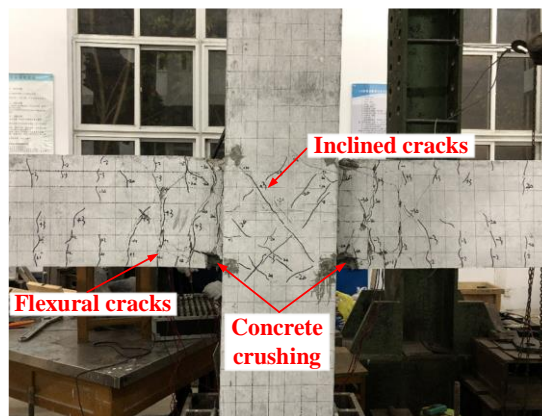
(b) ZJ-2



(c) ZJ-3



(d) ZJ-4



(e) XJ-1

357
358

359
360

361
362

363 **Fig. 11.** Final failure modes and overall crack patterns for the (a) ZJ-1, (b) ZJ-2, (c) ZJ-3, (d) ZJ-4, (e) XJ-1
364 joints.

365 **3.5. Ductility**

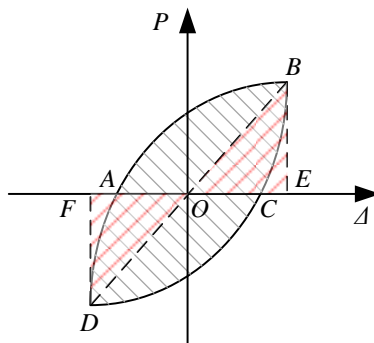
366 The displacement ductility ratio $\mu (= \Delta_u / \Delta_y)$ is defined as the ratio of the horizontal ultimate
367 displacement Δ_u to the horizontal yield displacement Δ_y . Table 5 lists the displacement ductility
368 ratio μ for the test specimens. The average displacement ductility ratio of joints ZJ-1, ZJ-2, ZJ-
369 3, ZJ-4 and XJ-1 are 2.82, 2.67, 2.79, 2.87 and 3.03, respectively, indicating that they have
370 sufficient deformation capacity for seismic applications [24]. Compared with joint XJ-1, the
371 average displacement ductility ratios of joints ZJ-1, ZJ-2 and ZJ-3 are reduced by 6.9%, 11.9%
372 and 7.9%, respectively. It may be attributed to the use of prestressed tendons, which increases
373 the overall stiffness, resulting in a reduction in horizontal ultimate displacement. The ductility
374 of specimens ZJ-2 and ZJ-3 is slightly lower than that of ZJ-1, indicating that increased effective
375 prestress established at the end of the beam and axial compression ratio reduce joint ductility
376 and deformation capacity. In comparison with specimen ZJ-1, the horizontal yield
377 displacements of specimens ZJ-2, ZJ-3, and ZJ-4 increase by 15.4%, 8.1% and 14.4%,
378 respectively, and the horizontal ultimate displacements by 9.5%, 7.0% and 16.2%. As can be
379 seen, the horizontal yield and ultimate displacements of the prestressed precast RC joints
380 assembled by steel sleeves increase with the increase of the axial compression ratio, effective
381 prestress established at the end of the beam and stirrup ratio, while the ductility decreases with
382 the increase of the axial compression ratio and effective prestress.

383

384 **3.6. Energy dissipation capacity**

385 The energy dissipation capacity of joints is an important index to assess their seismic
 386 performance. As shown in Fig. 12, the equivalent viscous damping ratio h_e formula is expressed
 387 as follows [32].

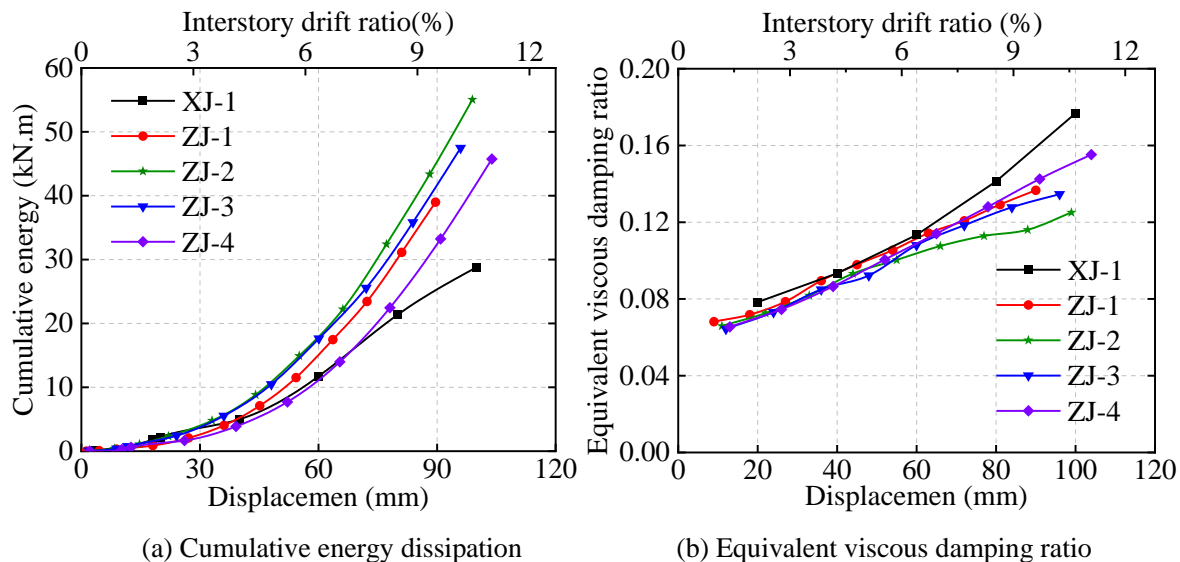
388
$$h_e = \frac{S_{ABCD}}{2\pi(S_{ODF} + S_{OBE})} \quad (1)$$



389
 390 **Fig. 12.** Definition of equivalent viscous damping ratio.

391 Fig. 13 shows the cumulative energy dissipation and equivalent viscous damping ratio h_e
 392 of the specimens tested. It can be seen that the cumulative energy dissipations of specimens ZJ-
 393 1, ZJ-2, ZJ-3, ZJ-4 and XJ-1 are 38.9 kN·m, 55.0 kN·m, 47.5 kN·m, 45.7 kN·m and 28.8 kN·m,
 394 respectively, achieving 1.3~1.9 higher energy dissipation than that of the cast-in-place RC joint.
 395 In the initial stage of the test, each specimen maintained a linear elastic behavior, and the
 396 equivalent viscous damping ratios were basically the same. However, with the increase of the
 397 plastic deformation, the equivalent viscous damping ratios of specimen ZJ-2 and specimen ZJ-
 398 3 decreased by 8.8% and 2.2%, respectively, compared with specimen ZJ-1, indicating that with
 399 the increase of axial compression ratio and prestress the hysteretic loop pinching effect of the
 400 joint is improved, and the axial compression ratio has a great influence. Under the same
 401 conditions, the equivalent viscous damping ratio of specimen ZJ-4 is 13.1% higher than that of
 402 specimen ZJ-1, and the cumulative energy dissipation is 17.5%, indicating that with the increase
 403 of stirrup ratio in the core area, the energy dissipation capacity of the joint is improved, and the
 404 hysteretic curve of the specimen becomes fuller. This is because the horizontal stirrup in the

405 core area of the joint inhibits the occurrence and development of concrete inclined cracks,
 406 subsequently, the development rate of failure of prestressed precast RC joints assembled by
 407 steel sleeves is reduced.



408
 409 (a) Cumulative energy dissipation (b) Equivalent viscous damping ratio
 410 **Fig. 13.** Energy dissipation of the specimens.

411 3.7. Stiffness degradation

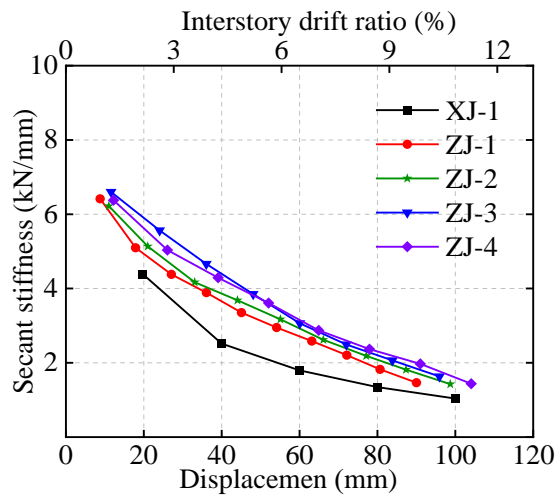
412 Stiffness degradation reflects the influence of damage evolution on the structure, which is
 413 one of the important characteristics of structural dynamic performance. In the low cycle
 414 repeated loading test, the stiffness coefficient K_i of the specimen is generally expressed by the
 415 secant stiffness of the skeleton curve [33]:

$$416 K_i = \frac{|+P_i| + |-P_i|}{|+\Delta_i| + |-\Delta_i|} \quad (2)$$

417 where $+P_i$ and $-P_i$ are the i -th positive and negative horizontal peak load, and $+\Delta_i$ and $-\Delta_i$ are the
 418 displacements corresponding to the i -th positive and negative horizontal peak loads.

419 Fig. 14 illustrates the relationship between secant stiffness and horizontal displacement of
 420 the test specimens in each cycle. The secant stiffness K_i of the prestressed precast RC joints
 421 assembled by steel sleeves is significantly greater than that of the cast-in-place RC joint due to
 422 the prestressed tendons effect. At the initial stage of loading, the secant stiffness K_i of specimens
 423 ZJ-3 and ZJ-4 is higher than that of specimens ZJ-1 and ZJ-2. With the continuous increase of

424 horizontal loading displacement, the secant stiffness K_i of each specimen gradually decreases
 425 and, subsequently, the difference in stiffness of each joint gradually decreases. The comparison
 426 shows that the stiffness degradation rate of the specimen gradually increases with the increase
 427 of the prestress level. In addition, the stiffness degradation rate of the specimen gently decreases
 428 with the increase or decrease of the stirrup ratio in the core area of the joint. Therefore, the
 429 increase of effective prestress established at the end of the beam and stirrup ratio in the core
 430 area of the joint can effectively improve the initial stiffness of the prestressed precast RC joint
 431 assembled by steel sleeves, while the effect of the axial compression ratio is neglectable.
 432 However, the secant stiffness K_i of each specimen has little difference at the failure stage.



433
 434 **Fig. 14.** Stiffness degradation curves of the specimens.

435 3.8. Deformation recovery performance

436 The deformation recovery capacity of structures directly affects their seismic performance,
 437 repairability, and repair cost. The deformation recovery capacity is usually expressed by the
 438 residual deformation rate μ_r :

$$439 \mu_r = \frac{\Delta_r}{\Delta_u} \quad (3)$$

440 where Δ_r and Δ_u are the horizontal residual deformation displacement and horizontal ultimate
 441 displacement of the specimen, respectively. The calculated results are shown in Table 6. As can
 442 be seen, the average residual deformation rate of prestressed precast RC joints ranges from 20.2%

443 to 32.4%, whereas the average residual deformation rate of cast-in-place joint XJ-1 is 55.4%.
 444 Meanwhile, comparing the test results of specimens ZJ-1 to ZJ-4, the residual deformation rate
 445 of specimen ZJ-4 is lower than that of specimen ZJ-1, and the horizontal residual displacements
 446 are similar, mainly because the increase of stirrup ratio increases the horizontal peak load and
 447 horizontal ultimate displacement of specimen ZJ-4, thus the stirrup ratio has less effect on the
 448 horizontal residual displacement. In addition, with the increase of prestress level, the residual
 449 deformation rate of the joint gradually decreases, and the self-centring ability gradually
 450 increases. When the axial pressure is relatively smaller, the self-centring ability of the
 451 prestressed precast RC joint assembled by steel sleeves is better.

452 **Table 6** Residual deformation rate of specimens

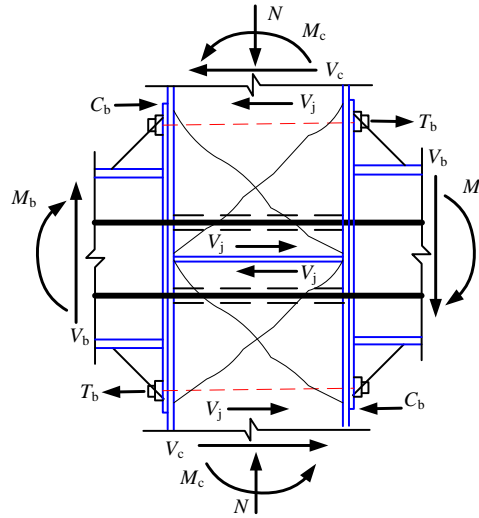
Specimen	Δ_r (mm)		Δ_u (mm)		μ_r (%)		μ_r (%) average
	+	-	+	-	+	-	
ZJ-1	23.2	25.0	90.0	90.1	25.8	27.7	26.8
ZJ-2	29.8	34.6	98.1	98.9	30.4	34.4	32.4
ZJ-3	19.9	19.0	96.0	96.6	20.7	19.7	20.2
ZJ-4	23.6	22.4	104.1	105.1	22.1	21.3	21.7
XJ-1	54.9	58.9	100.1	99.9	54.8	56.0	55.4

453

454 **4. Shear capacity prediction of proposed joints**

455 As can be observed in the physical testing, the longitudinal reinforcement and steel sleeve
 456 did not yield, and the failure mode of the prestressed precast RC joint assembled by steel sleeves
 457 was mainly manifested by concrete crushing in the core area of the joints and yielding of stirrups.
 458 Therefore, the force mechanism of the prestressed precast RC joint assembled by steel sleeves
 459 may be represented by the diagonal compression strut model, considering only the contribution
 460 of the concrete's compression strut to the bearing capacity. The load transfer of the prestressed
 461 precast RC joint assembled by steel sleeves is shown in Fig. 15. The shear capacity in the core
 462 area of the prestressed precast RC joint assembled by steel sleeves is obtained from the

463 equilibrium equation below:



464

465 **Fig. 15.** Mechanical behavior of prestressed precast RC joint assembled by steel sleeves.

466

$$V_j = \frac{\sum M_b}{h_b} \left(1 - \frac{h_b}{H_c - h_b} \right) \quad (4)$$

467 where V_j is the joint shear capacity, h_b is the height of the beam section, H_c is the height of the
 468 column, and M_b is the bending moment of the beam, V_b is the vertical shear force of the column
 469 at the steel sleeve, C_b is horizontal shear forces of the column at the stiffeners, T_b is the
 470 horizontal tension transmitted from the bolt to the column.

471 According to the diagonal compression strut model [34], the joint shear capacity V_j is
 472 expressed in the following equation (5).

$$V_j = f_c A_c \cos \theta \quad (5)$$

$$A_c = a_s b_s \quad (6)$$

$$a_s = \sqrt{a_b^2 + a_c^2} \quad (7)$$

$$a_c = \alpha_1 \left(1 + \xi_1 \frac{N}{f_c b_c h_c} \right) h_j \quad (8)$$

477 where f_c is the axial compressive strength of concrete; A_c is the effective cross-sectional area of
 478 the diagonal compression strut; θ is the angle between the diagonal compression strut and the

479 horizontal axis; a_s is the height of the diagonal compression strut [35], a_b and a_c are the heights
 480 of the compressive zones of the beam and column sections, respectively [36]; N is the axial load
 481 at the column end; h_j is the effective height of the joint core area; b_c and h_c are the cross-sectional
 482 dimensions of the column; ζ_1 is the softening factor of the compressive strength of concrete; α_1
 483 is the influence factor obtained from Eq. (8).

484 The shear capacity of RC beam-column joints in GB50010-2010 [27] is given by Eq. (9):

$$485 \quad V_{jGB} = 0.1\eta_j \left(1 + \frac{N}{b_c h_c f_c}\right) f_c b_j h_j + f_{vy} \frac{A_{svj}}{s} (h_0 - a'_s) \quad (9)$$

486 where η_j is the cross beam restraint influence coefficient, b_j is the effective width of the joint
 487 core area; f_{vy} is stirrup tensile strength; A_{svj} is the area of stirrups in the core area of the joint; s
 488 is the distance of horizontal stirrup in the joint core region; h_0 is the effective height of beam
 489 section; a'_s is the distance from the joint point of the beam compressive reinforcement to the
 490 concrete compressive edge.

491 The shear capacity of the core area of the joint in American code ACI 318-19 [37] is
 492 obtained from Eq. (10):

$$493 \quad V_{jACI} = 0.083\gamma\sqrt{f_c} b_j h_j \quad (10)$$

494 where γ is the influence coefficient of beam-column joint type. When the joint core area is
 495 connected to the beam on three or two sides, γ is 15 [38]. The shear capacity of the core area of
 496 the joint was not only related to the strength of concrete and stirrups, but also related to the
 497 effective prestress established at the end of the beam. Combined with relevant experimental
 498 research [39], the calculation formula of the effect of effective prestress established at the end
 499 of the beam on the shear capacity was obtained, as shown in formula (11):

$$500 \quad V_p = 0.05N_p \quad (11)$$

501 where V_p is the shear capacity provided by the effective prestress established at the end of the
502 beam; N_p is the effective prestress of the prestressed tendons. On the basis of the shear capacity
503 of the core area of the joint calculated by the diagonal compression strut model [34], GB50010-
504 2010 [27], and ACI 318-19 [37], the modified shear capacity calculation formulas of the
505 prestressed precast RC joint assembled by steel sleeves are given by Eqs. (12) to (14).

$$506 \quad V'_{jDSM} = f_c A_c \cos \theta + 0.05 N_p \quad (12)$$

$$507 \quad V'_{jGB} = 0.1 \eta_j \left(1 + \frac{N_c}{b_c h_c f_c} \right) f_c b_j h_j + f_{vy} \frac{A_{suj}}{s} (h_0 - a'_s) + 0.05 N_p \quad (13)$$

$$508 \quad V'_{jACI} = 0.083 \gamma \sqrt{f_c} b_j h_j + 0.05 N_p \quad (14)$$

509 Table 7 shows the comparison of the predicted and experimental shear capacity values, AV
510 and CoV represent the average value and coefficient of variation, respectively. The average
511 ratio of predicted values to test values in Eqs. (12), (13) and (14) are 0.91, 0.86 and 0.94,
512 respectively, while the coefficients of variation are 0.082, 0.032 and 0.027, respectively. The
513 ACI prediction (Eq. (14)) shows a good agreement with the test results, with minimum
514 discreteness and less than the test value, which tended to be safe and reliable.

515 **Table 7** Shear strength capacity of specimens

specimen	V_j /kN	V'_{jDSM} /kN	V'_{jDSM}/V_j	V'_{jGB} /kN	V'_{jGB}/V_j	V'_{jACI}	V'_{jACI}/V_j
ZJ-1	643.5	581.8	0.90	561.9	0.87	633.6	0.98
ZJ-2	685.3	711.1	1.03	607.0	0.89	634.6	0.93
ZJ-3	697.0	596.3	0.86	576.3	0.83	648.1	0.93
ZJ-4	731.7	623.8	0.85	603.8	0.83	675.6	0.92
AV	—	—	0.91	—	0.86	—	0.94
CoV	—	—	0.082	—	0.032	—	0.027

516

517 **5. Conclusions**

518 The cyclic loading tests of four prestressed precast RC beam-column joints assembled by

519 steel sleeves and one cast-in-place counterpart were carried out to study their seismic
520 performance. The main conclusions are summarized as follows.

521 (1) Compared with the traditional cast-in-place RC joints, the residual deformation of the
522 proposed prestressed precast RC joints assembled by steel sleeves is small, exhibiting good
523 self-centring ability and high bearing capacity, confirming reliability and efficiency of the
524 proposed joint.

525 (2) The axial compression ratio and effective prestress have a great influence on the energy
526 dissipation capacity of the prestressed precast RC joint assembled by steel sleeves. With the
527 increase of the axial compression ratio and effective prestress of prestress tendon, the energy
528 dissipation capacity gradually increases.

529 (3) With the increase of the effective prestress of prestressed precast RC joint assembled
530 by steel sleeves and stirrup ratio in the core area of the joint, the initial stiffness of the joint is
531 effectively improved, but the effect of the axial compression ratio is limited. For prestressed
532 precast RC joints assembled by steel sleeves, the horizontal yield and ultimate displacements
533 increase with the increase of axial compression ratio, stirrup ratio and effective prestress of
534 prestress tendon.

535 (4) Based on the shear mechanism of the prestressed precast RC joint assembled by steel
536 sleeves core area, combined with the calculation formulae of GB 50010 and ACI 318, formulae
537 for the shear capacity of prestressed precast RC joint assembled by steel sleeves were developed,
538 showing good agreement with the experimental results.

539 **Acknowledgments**

540 The authors would like to thank the financial support provided by the Natural Science

541 Foundation of Jiangsu Province, China (BK20201436), the Open Foundation of Jiangsu
542 Province Engineering Research Center of Prefabricated Building and Intelligent Construction
543 (2021), the Blue Project Youth Academic Leader of Colleges and Universities in Jiangsu
544 Province (2020) and the Postgraduate Research & Practice Innovation Program of Jiangsu
545 Province, China (KYCX21_3225).

546 **Notations**

547 N : Axial load at the column end

548 N_y : Yield strength of the entire column section

549 Δ_y : Horizontal yield displacement

550 P_y : Horizontal yield load

551 P_m : Positive peak bearing capacity

552 K_i : Stiffness coefficient

553 $+P_i$: i -th positive horizontal peak load

554 $-P_i$: i -th negative horizontal peak load

555 $+\Delta_i$: Displacements corresponding to the i -th positive horizontal peak loads

556 $-\Delta_i$: Displacements corresponding to the i -th negative horizontal peak loads

557 μ : Displacement ductility ratio

558 μ_r : Residual deformation rate

559 Δ_r : Horizontal residual deformation displacement

560 Δ_u : Horizontal ultimate displacement

561 h_e : Equivalent viscous damping ratio

562 f_c : Concrete strength

563 V_c : Shear capacity

564 f_{ptk} : Ultimate strength of the prestressed tendon

565 V_j : Joint shear strength capacity

566 h_b : Height of the beam section

567 H_c : Height of the column

568 M_b : Bending moments of the beam

569 V_b : Vertical shear force of the column at the steel sleeve

570 C_b : Horizontal shear forces of the column at the stiffeners

571 T_b : Horizontal tension transmitted from the bolt to the column

572 A_c : Effective cross-sectional area of the diagonal compression strut

573 θ : Angle between the diagonal compression strut and the horizontal axis

574 a_s : Height of the diagonal compression strut

575 a_b : Height of the compressive zones of the beam section

576 a_c : Height of the compressive zones of the column section

577 h_j : Effective height of the joint core area

578 b_c : Width of the column section

579 h_c : Height of the column section

580 ζ_1 : Softening factor of the compressive strength of concrete

581 α_1 : Influence factor

582 η_j : Cross beam restraint influence coefficient

583 b_j : Effective width of the joint core area

584 f_{yv} : Stirrup tensile strength

585 A_{svj} : Area of stirrups
586 h_0 : Effective height of beam section
587 s : Distance of horizontal stirrup in the joint core region
588 a'_s : Distance from the joint point of the beam compressive reinforcement to the concrete
589 compressive edge
590 γ : Influence coefficient of beam-column joint type
591 V_p : Shear capacity provided by effective prestress established at the end of the beam
592 N_p : Effective prestress of the prestressed tendons

593 **References**

- 594 [1] Gao Q, Li JH, Qiu ZJ, Hwang HJ. Cyclic loading test for interior precast SRC beam-column
595 joints with and without slab. *Engineering Structures* 2019;182:1-12.
- 596 [2] Savoia M, Buratti N, Vincenzi L. Damage and collapses in industrial precast buildings after
597 the 2012 Emilia earthquake. *Engineering Structures* 2017;137:162-80.
- 598 [3] Li S, Li Q, Zhang H, Jiang H, Yan L, Jiang W. Experimental study of a fabricated confined
599 concrete beam-to-column connection with end-plates. *Construction and Building Materials*
600 2018;158:208-216.
- 601 [4] Huang W, Hu G, Miao X, Fan Z. Seismic performance analysis of a novel demountable
602 precast concrete beam-column connection with multi-slit devices. *Journal of Building*
603 *Engineering* 2021;44:102663.
- 604 [5] Li X, Zhang J, Liu B, Jiang H, Min X. Bond stress distribution analysis between non-
605 prestressed steel strand and concrete in novel beam-to-column connection. *Engineering*
606 *Structures* 2021;242:112523.
- 607 [6] Xue W, Hu X, Ren D, Hu X. Hysteretic performance of precast beam-column connections
608 fabricated with high-strength materials. *Structures* 2021;33:4568-4578.

- 609 [7] Yu J, Zhang W, Tang Z, Guo X, Pospíšil S. Seismic behavior of precast concrete beam-
610 column joints with steel strand inserts under cyclic loading. *Engineering Structures*
611 2020;216:110766.
- 612 [8] Kurama YC, Sritharan S, Fleischman RB, Restrepo JI, Henry RS, Cleland NM et al.
613 Seismic-resistant precast concrete structures: state of the art. *Journal of Structural Engineering*
614 2018;144(4):03118001.
- 615 [9] Yan Q, Chen T, Xie Z. Seismic experimental study on a precast concrete beam-column
616 connection with grout sleeves. *Engineering Structures* 2018;155:330-344.
- 617 [10] Zhong Y, Xiong F, Chen J, Deng A, Chen W, Zhu X. Experimental study on a novel dry
618 connection for a precast concrete beam-to-column joint. *Sustainability* 2019;11:1-22.
- 619 [11] Zhang J, Ding C, Rong X, Yang H, Li Y. Development and experimental investigation of
620 hybrid precast concrete beam-column joints. *Engineering Structures* 2020;219:110922.
- 621 [12] Korkmaz HH, Tankut T. Performance of a precast concrete beam-to-beam connection
622 subject to reversed cyclic loading. *Engineering Structures* 2005;27(9):1392-1407.
- 623 [13] Kim JH, Choi S-H, Hwang J-H, Jeong H, Han S-J, Kim KS. Experimental study on lateral
624 behavior of post-tensioned precast beam-column joints. *Structures* 2021;33:841-854.
- 625 [14] Cai X, Pan Z, Zhu Y, Gong N, Wang Y. Experimental and numerical investigations of self-
626 centering post-tensioned precast beam-to-column connections with steel top and seat angles.
627 *Engineering Structures* 2021;226:111397.
- 628 [15] Cai X, Gong N, Fu CC, Zhu Y, Wu J. Seismic behavior of self-centering prestressed precast
629 concrete frame subassembly using steel top and seat angles. *Engineering Structures*
630 2021;229:111646.

- 631 [16] Vidjeapriya R, Jaya KP. Experimental study on two simple mechanical precast beam-
632 column connections under reverse cyclic loading. *Journal of Performance of Constructed*
633 *Facilities* 2013;27(4):402-414.
- 634 [17] Erats O, Ozden S, Ozturan T. Ductile connections in precast concrete moment resisting
635 frames. *Pci Journal* 2006;51(3):66-76.
- 636 [18] Nakaki SD, Englekirk RE, Plaehn JL. Ductile connectors for a precast concrete frame. *Pci*
637 *Journal* 1994;39(4):46-59.
- 638 [19] Englekirk RE. Development and testing of a ductile connector for assembling precast
639 concrete beams and columns. *Pci Journal* 1995;40(2):36-51.
- 640 [20] Liu Y, Guo Z, Ding J, Wang X, Liu Y. Experimental study on seismic behaviour of plug-
641 in assembly concrete beam-column connections. *Engineering Structures* 2020;221:111049.
- 642 [21] Choi HK, Choi YC, Choi CS. Development and testing of precast concrete beam-to-
643 column connections. *Engineering Structures* 2013;56:1820-1835.
- 644 [22] Bai J, He J, Li C, Jin S, Yang H. Experimental investigation on the seismic performance
645 of a novel damage-control replaceable RC beam-to-column joint. *Engineering Structures*
646 2022;267:114692.
- 647 [23] Unal M, Burak B. Development and analytical verification of an inelastic reinforced
648 concrete joint model. *Engineering Structures* 2013;52:284-294.
- 649 [24] GB 50011-2010. Code for seismic design of buildings. Beijing, China: China Architecture
650 and Building Press; 2010.
- 651 [25] JGJ 138-2016. Code for design of composite structures. Beijing, China: China Architecture
652 and Building Press; 2016.

- 653 [26] GB 50017-2010. Code for design of steel structures. Beijing, China: China Architecture &
654 Building Press; 2010.
- 655 [27] GB 50010-2010. Code for design of concrete structures. Beijing, China: China
656 Architecture & Building Press; 2010.
- 657 [28] GB/T 50081-2019. Standard for test methods of concrete physical and mechanical
658 properties. Beijing, China: China Architecture & Building Press; 2010.
- 659 [29] GB/T 228.1-2021. Metallic materials-tensile testing-part 1: Method of test at room
660 temperature. Beijing, China Architecture & Building Press; 2021.
- 661 [30] JGJ/T101-2015. Specification for the seismic test of buildings. Beijing, China: China
662 Architecture & Building Press; 2015.
- 663 [31] Zhang J, Pei Z, Rong X, Zhang X. Experimental study of HSS-reinforced exterior beam–
664 column joints with different enhancement details. *Engineering Structures* 2021;246:113038.
- 665 [32] Ghayeb HH, Razak HA, Sulong RNH. Seismic performance of innovative hybrid precast
666 reinforced concrete beam-to-column connections. *Engineering Structures* 2020;202:109886.
- 667 [33] Kulkarni SA, Li B, Yip WK. Finite element analysis of precast hybrid-steel concrete
668 connections under cyclic loading. *Journal of Constructional Steel Research*. 2008;64(2):190-
669 201.
- 670 [34] Hwang SJ, Lee HJ. Analytical model for predicting shear strengths of interior reinforced
671 concrete beam-column joints for seismic resistance. *Structural Journal* 2000;97(1):35-44.
- 672 [35] Hwang SJ, Lee HJ. Analytical model for predicting shear strengths of exterior reinforced
673 concrete beam-column joints for seismic resistance. *ACI Structural Journal* 1999;96:846-857.
- 674 [36] Paulay T, Priestley MNJ. *Seismic design of reinforced concrete and masonry buildings*.

675 New York: John Wiley & Sons; 1992. p. 210-239.

676 [37] ACI Committee 318. Building code requirements for structural concrete and commentary.
677 ACI 318-19, American Concrete Institute, Farmington Hills, MI, USA; 2019.

678 [38] Ma F, Deng M, Yang Y. Seismic experimental study on a UHPC precast monolithic
679 concrete beam-column connection. *Engineering Mechanics* 2021;38(10):90-102. [in Chinese].

680 [39] Tang J, Chen J, Hua X. Analysis of shear bearing capacity of prestressed concrete frame
681 joints. *Building Structure* 1992;7(1):20-26. [in Chinese].